SUPPORTING INFORMATION

Impact of antigen density on recognition by monoclonal antibodies

Laure Bar,[†] Jérôme Dejeu,[†] Rémy Lartia,[†] Fouzia Bano,[‡] Ralf P. Richter,[‡] Liliane Coche-Guérente[*†] and Didier Boturyn[*†]

[†]Univ. Grenoble-Alpes, CNRS, DCM UMR 5250, F-38000 Grenoble, France

[‡]University of Leeds, School of Biomedical Sciences, Faculty of Biological Sciences, School of Physics and Astronomy, Faculty of Engineering and Physical Sciences, Astbury Center for Structural Molecular Biology, and Bragg Centre for Materials Research, Leeds, United Kingdom

Corresponding Author:

[*] E-mail: didier.boturyn@univ-grenoble-alpes.fr.

Table of Contents:

1. General procedure for CD20 synthesis

1.1. Reagents and material

All Fmoc amino acid derivatives and resins were purchased from Advanced ChemTech Europe (Brussels, Belgium), Bachem Biochimie SARL (Voisins-Les-Bretonneux, France) and France Biochem S.A. (Meudon, France). Other reagents were obtained from Aldrich (Saint Quentin Fallavier, France) or Acros (Noisy-Le-Grand, France). RP-UHPLC analyses were performed on Waters equipment consisting of a Waters Acquity H-Class Bio UPLC combined to a Waters SQ Detector 2 mass spectrometer. The analytical column used was a ACQUITY UPLC BEH C18 Column, 130Å, 1.7 µm, 2.1 mm x 50 mm operated at 0.6 mL/min with linear gradient programs in 2.20 min run time (routine program: 5% to 100 % B in 2.20 min). UV monitoring was performed at 214 nm. Solvent A consisted of H2O containing 0.1% trifluoroacetic acid (TFA) and solvent B consisted of CH3CN containing 0.1% TFA. Water was of Milli-Q quality. CH3CN and TFA were LC-MS grade. RP-HPLC purifications were performed on Gilson GX-281 or GX-281. The preparative column, Macherey-Nagel 100 Å 7 µm C18 particles, 250 × 21 mm was operated at 20.84 mL/min. Solvents A and B were the same as the ones used in RP-HPLC analysis.

1.2. Synthesis of CD20

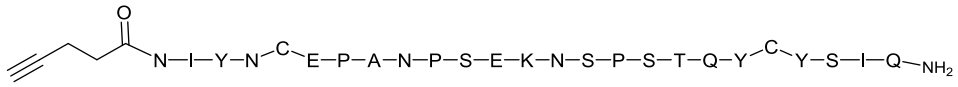

Synthesis of the protected peptide was carried out using the Fmoc/*t*-Bu strategy. For both peptides, the first amino-acid was manually attached on a 2-chlorotritylchloride® resin (loading ≈ 0.5 mmol/g). Peptides were then elongated on a peptide synthesizer. Coupling reactions were performed by using 4 eq. of *N*-Fmoc-protected amino acid (relative to the resin loading) activated *in situ* with 2 equiv. of HBTU and 3-5 eq. of diisopropylethylamine (DIPEA) in DMF (10 mL/g resin) for 30 min. *N*-Fmoc protecting groups were removed by treatment with a piperidine/DMF solution (1:4) for 10 min (10 mL/g resin). The alkyne function was then manually added on N-terminus by a coupling reaction with 4-Pentynoic acid (2 equiv.). The linear peptides were then released from the resin by treatments with a solution of trifluoroacetic acid/trisisopropylsilane/H_2O/2,2′-(Ethylenedioxy)diethanethiol (92.5/2.5/2.5/2.5, 10 mL/mg resin, 1 h). With this treatment, all protecting group of the peptides are removed. After evaporation, diethyl ether was added to precipitate peptides. They were then triturated and washed three times with diethyl ether to obtain crude materials.

1.3. Disulfide bond formation

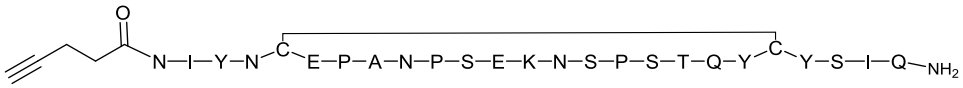

Disulfide bonds were formed by diluting peptides to 500 µM in Tris buffer 0.1 M, guanidine 20 mM, and DMSO 5% (v:v) and maintaining oxidative conditions for 48 h. Disulfide bond formation was checked by RP-UHPLC analyses.

Peptides were then purified by RP-HPLC and their concentration quantified with a UV spectrophotometer.

UPLC analysis of CD20:

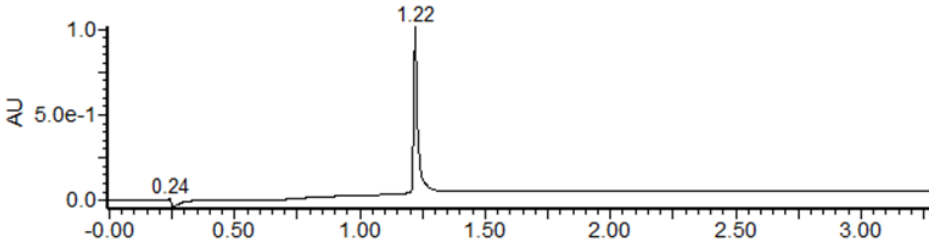

ESI analysis of CD20:

MS (ESI-MS, positive mode): $C_{126}H_{183}N_{33}O_{44}S_2$ Calcd : MW = 2928.264 g.mol^{-1} ; Found MW = 2928.22 g.mol^{-1}

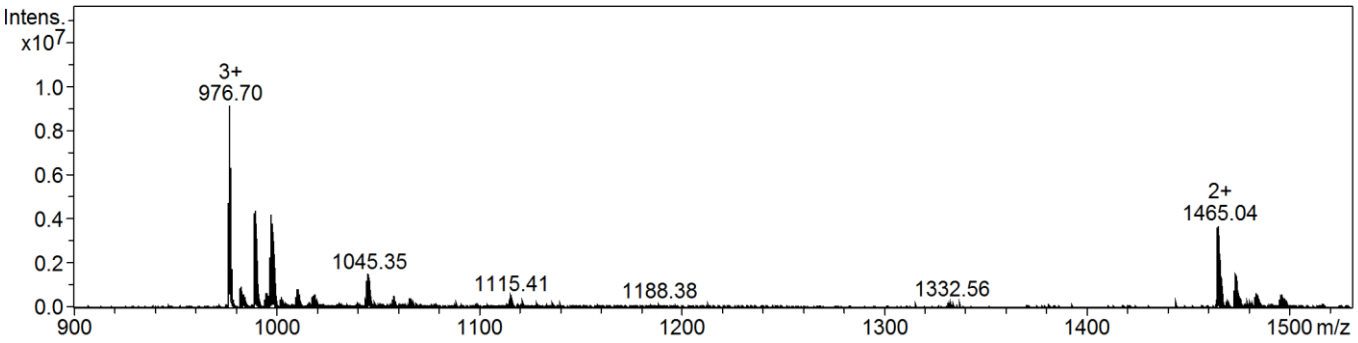

2. SPR quantification of grafted peptide

2.1. Jung's formula

Surface Plasmon resonance (SPR) is an optical sensing technique which, similar to SE, is sensitive to changes in refractive index. We considered here a multilayer structure with the first layer SAM used to subsequently attach CD20 epitope considered as a second layer that has been monitored by SPR. The Jung's formula [1] combined with the De Feijter's equation (Eq. S1) allowed the conversion of the magnitude of the response units measured during the chemical coupling (conventionally expressed in RU) into areal mass densities Γ (in mol.cm^{-2}) as previously reported (Eq. S1): [2]

$$\Gamma = 10^{-6} RU . \frac{d'}{dn/dc} \frac{1}{e^{-d/dp}\left(1 - e^{-d'/dp}\right)} \qquad \text{(Eq. S1)}$$

where RU is the number of resonance units gained by the peptide grafting, d' is the thickness of the peptide film (d' = 4.6 nm, as determined by SE), d is the thickness of the SAM (d = 2.5 nm, as determined by SE), dn/dc is the refractive index increment (*dn*/*dc* = 527 cm^3.mol^{-1} which corresponds to 0.18 x 2928 for CD20), and *dp* is the evanescent wave depth (*dp* = 175 nm).[3]

This expression requires knowledge of SAM and CD20 layer thicknesses. The SPR response would be the same as that of the simple case of a CD20 layer alone directly attached to gold surface, except that its magnitude is reduced by a factor e^{-d/d_p} due to the SAM underlayer. As the thickness of the SAM is very thin compared to the penetration depth (2.5 nm versus 175 nm), this factor is close to 1 and the response due to the attachment of the CD20 layer is unaffected by the presence of SAM layer between the metal and the CD20 layer.

2.2. SPR determination of CD20 epitope density

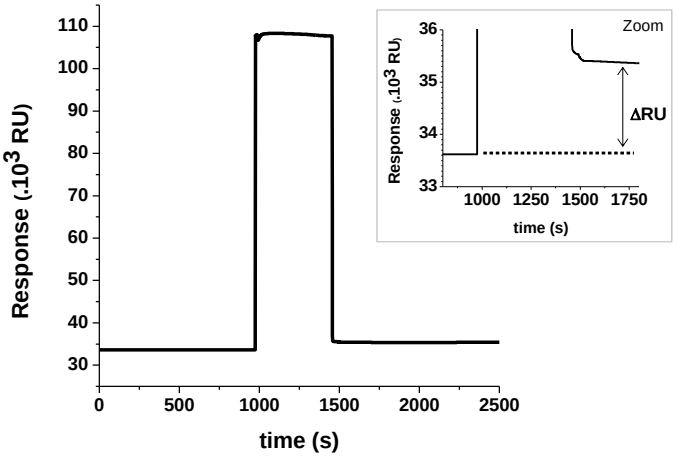

Figure S1. Determination of the number of resonance response units gained by the peptide grafting. The large change of refractive index during the injection of DMSO prevents the grafting to be monitoring in real-time. Therefore, the quantity of antigen immobilized on the surface is evaluated from the shift in resonance units after rinsing as compared to before peptide injection (ΔRU in the inset). On this example, the peptide was injected at 2 µl.min^{-1} for 480 s on a 20%-N_3 functionalized surface.

2.3. Correlation between the molar fraction of thiol-azide in the solution from which the SAMs were formed and the CD20 surface density.

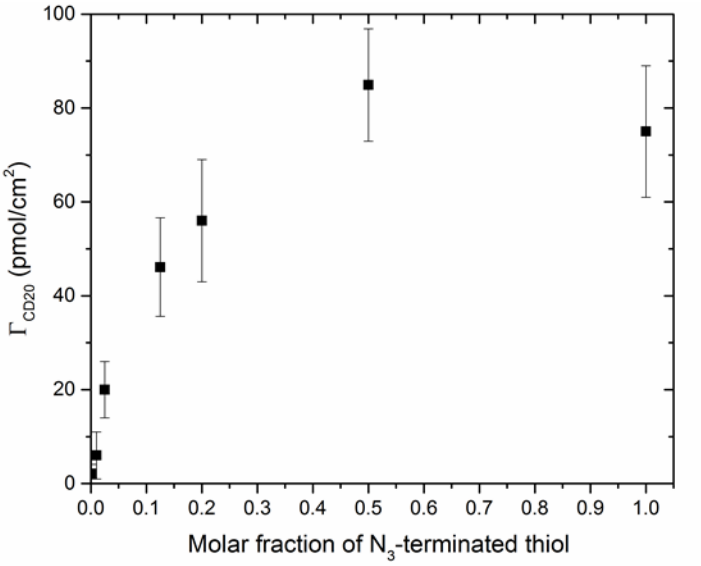

Figure S2. CD20 surface density (measured by the Jung's formula from SPR *in-situ* grafting) as a function of the molar fraction of N_3-terminated thiol in the thiol mixture used to prepare the SAMs.

Figure S2 shows that above 50% of thiol-azide CD20 surface density reached saturation. This observation could be explained by the size of CD20 (width max: 1.5 nm; length: 2.5 nm (non-stretched)). The theoretical saturation could be calculated from a densly packed layer of CD20 whose projected surface would be of 2.25 nm^2, such calculation leads to about 74 pmol/cm^2.

.

3. Optimization of SPR binding assays: Impact of buffer nature

The effect of buffer type on RTX binding to CD20 was studied since the rituximab is stored in an injectable rituximab solution (MabThera solution) that differs from the buffers we use routinely for SPR experiments. Binding assays were performed and compared in three buffer conditions (MabThera buffer, PBS buffer, or HEPES buffer) on the same surface. As can be seen on Figure S3, conventional buffers such as PBS or HEPES provided a better interaction. Consequently, we choose to work with PBS buffer after verifying the absence of dilution effect of MabThera buffer for the observed concentration range. A solution of 1 µM was prepared by diluting the RTX concentrated solution (MabThera solution of 69.5 µM) using 14.4 µL in 1000 µL of PBS.

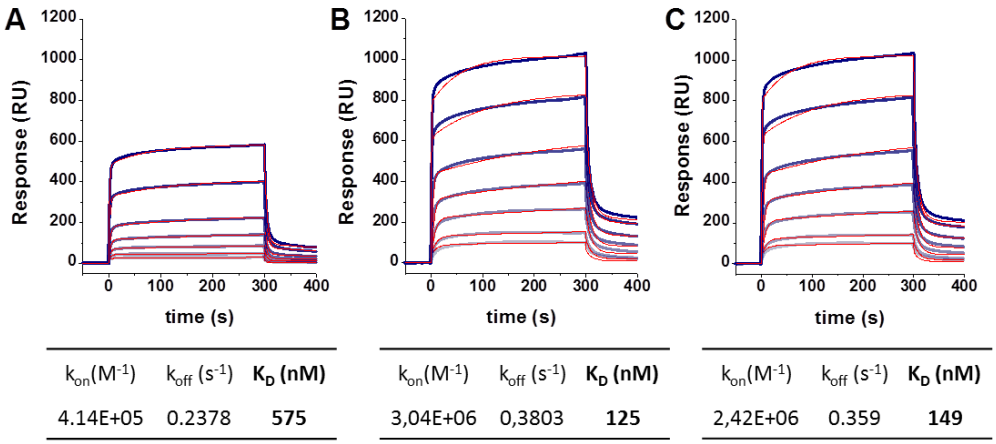

	$k_{on}(M^{-1})$	$k_{off}(s^{-1})$	K_D (nM)
A	4.14E+05	0.2378	**575**
B	3,04E+06	0,3803	**125**
C	2,42E+06	0.359	**149**

Figure S3. Binding assays performed by injecting rituximab antibody in different buffers. (A) in MabThera® Buffer = 154 mM NaCl, 25 mM citrate, 0.066% P80; (B) in PBS, 3 mM citrate, 0.005% P80; (C) in 10 mM Hepes, 150 mM NaCl, 3 mM citrate, 0.005% P80. Concentration range is: 10, 20, 50, 100, 200, 500, 1000 nM. These experiments were performed on the same surface functionalized with the ex-situ grafting protocol.

4. Specificity of CD20-functionalized surface toward RTX binding.

The graph below shows that trastuzumab (a mAb which belongs to the same IgG subclass) binds the CD20 functionalized surface in the same manner than on the CD20 scramble surface whatever the CD20 surface density.

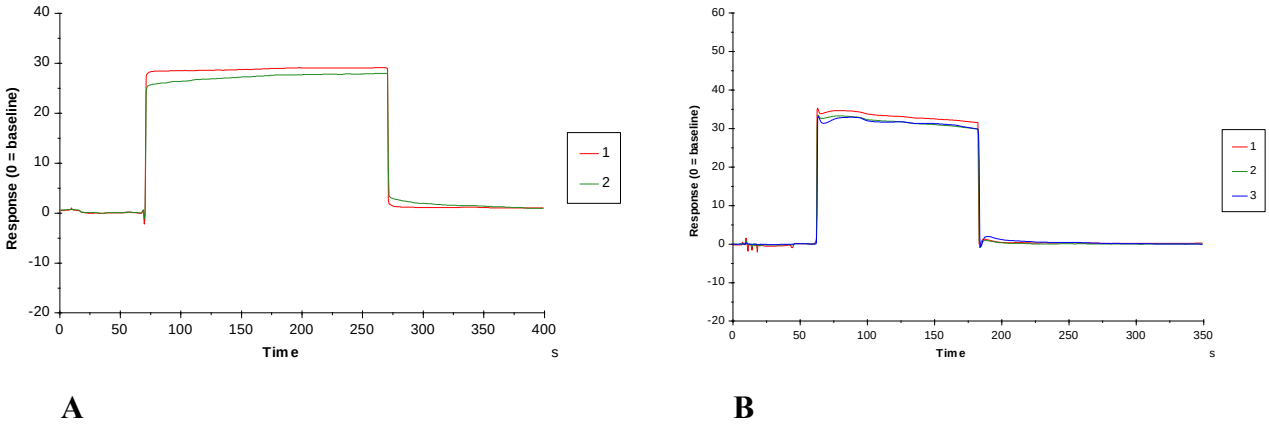

Figure S4. Overlapping of the sensorgrams characterizing the binding of trastuzumab (100 nM) on two different flow cells (Fc): Fc1 (red curve) CD20 scramble-functionalized surface, Fc2 (green curve) CD20-functionalized surface and Fc3 (blue curve) N_3-terminated SAM surface. Surface densities of CD20 or CD20 scramble functionalized surfaces correcpond to (A) 46 pmol.cm^{-2} (Fc1 and Fc2) and (B) 2.8 pmol.cm^{-2} (Fc1 and Fc2) and 0 pmol.cm^{-2} (Fc3).

Figures S4 shows that non-specific absorption of trastuzumab is similar on both CD20 and CD20 scramble surfaces at different densities.

5. Stability of the surface over time

CD20-coated SPR sensor chips were typically used for a large numbers of binding assays, each followed by a regeneration step. To confirm the stability of the CD20 coating over time, a standardized binding assay with 1 µM rituximab was performed at regular intervals. Figure S3 shows the responses corresponding to rituximab binding on a freshly prepared surface (black curve; R_{max} = 2550 RU), after 76 regeneration steps (purple curve; 2400 RU, or 94% of the initial response), and after 140 regeneration steps (blue curve; 2265 RU, or 89% of the initial response). These results confirm that the surface is stable over time, and that the loss of ligand activity was negligibly small over the duration of a binding assay.

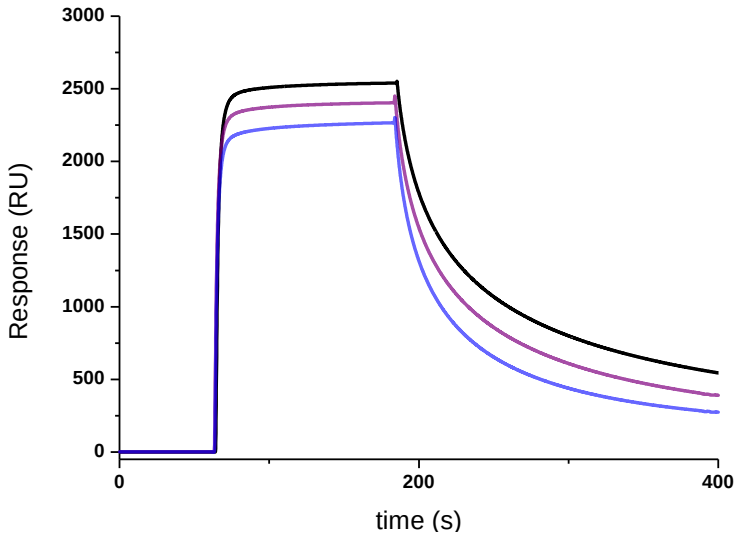

Figure S5. SPR signals obtained for a 1 µM rituximab injection on the same surface at different wear stages: freshly prepared surface (black), after 76 regeneration steps (purple), after 140 regeneration steps (blue). A regeneration step consist of an injection of Glycine/HCl solution, pH 2, for 10 s at 30 µl,min^{-1}.

6. Choice of the SPR model

The SPR data were fitted using a heterogeneous ligand (HL) model. The SPR response can be considered as a result of the contribution of two different independent interactions. One example of the deconvolution of the modelled signal is shown in figure S4. It appears that the two interactions exhibit very different magnitude, the second one is very weak and the curve shape is characteristic of a non-specific interaction with a continuous positive drift during the association phase without apparent dissociation phase. For the HL model, the data evaluation software provides two association rate constants, k_{on1} and k_{on2}, and two dissociation rate constants, k_{off1} and k_{off2}, as well as two theoretical maximal responses, R_{max1} and R_{max2}. These sets of parameters consist of the specific interaction (1st interaction in Figure S6; typically representing between 80 and 90% of the total SPR signal, see Figure S7A) and a non-specific interaction (2nd interaction in Fig. S6; representing the remaining signal of less than 20% in most cases). Consequently, the data presented in the manuscript are only related to the specific first interaction.

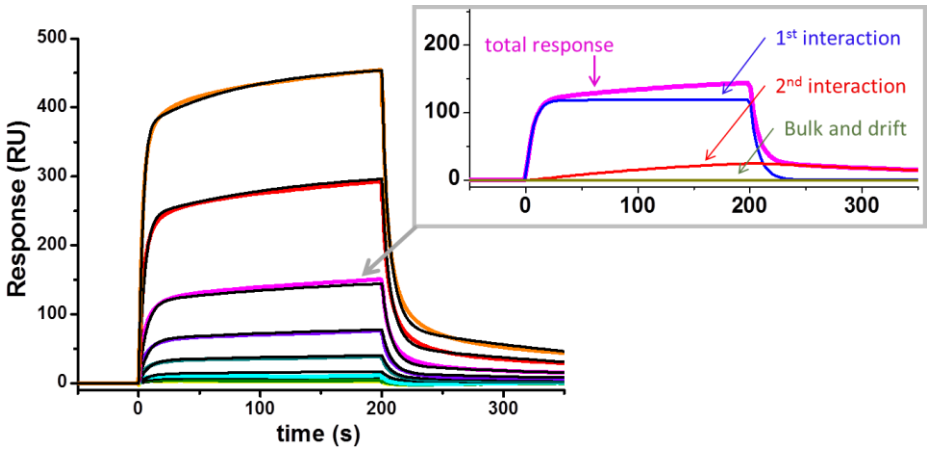

Figure S6. RTX-CD20 SPR binding profile obtained at 85 pmol.cm^{-2} of CD20 surface density. RTX concentrations were 5, 10, 20, 50, 100, 200, 500 and 1000 nM. The sensorgrams were fitted with the heterogeneous ligand kinetic model and the fitted curves were added to the graph (black curves). Insert: Signal deconvolution of the curve corresponding to the RTX injection of 500 nM. The observed sensorgram (pink) is composed of signal contributions of the specific interaction (1st interaction – blue curve) and a non-specific interaction (2nd interaction – red curve). Bulk and drift (=0) is represented by the green curve. By using the heterogeneous ligand model, we assume that each curve can be divided into two contributions. The experimental response (pink curve) is composed of a large SPR signal having the shape of a specific binding (1st interaction – blue curve) and a second weak SPR signal whose shape is characteristic of a non-specific binding (2nd interaction – red curve).

For the example presented in Figure S5, the numeric contribution of each interaction is given by the fitted R_{max} values (Table S1). With R_{max1} = 804 and R_{max2} = 127 RU, the interaction associated to the blue curve represents 84 % of the SPR response, and strengthens the idea that this corresponds to the specific interaction.

Table S1. Parameters of the CD20/RTX interaction obtained after curve fitting. The heterogeneous ligand model provides two sets of data corresponding to interaction 1 (blue curve) and interaction 2 (red curve).

k_{on1} (1/Ms)	k_{off1} (1/s)	K_{D1} (M)	R_{max1} (RU)	k_{on2} (1/Ms)	k_{off2} (1/s)	K_{D2} (M)	R_{max2} (RU)	RI (RU)	χ^2 (RU²)
6.72E+05	0.7668	1.14E-06	804	8263	0.003825	4.63E-07	127	0	7.66

Normalized maximal responses R_{max} of the two interactions are presented in Figure S7A. It shows that the signal magnitude of the second interaction is in the minority (in most cases, it represents less than 20% of the total signal magnitude). The association rate constants k_{on} for the two interactions as a function of CD20 surface coverage are shown in Figure S5B. kon values related to the second interaction are typically much smaller than for the first interaction, and the variation in kon2 is low across the full range of CD20 surface densities.

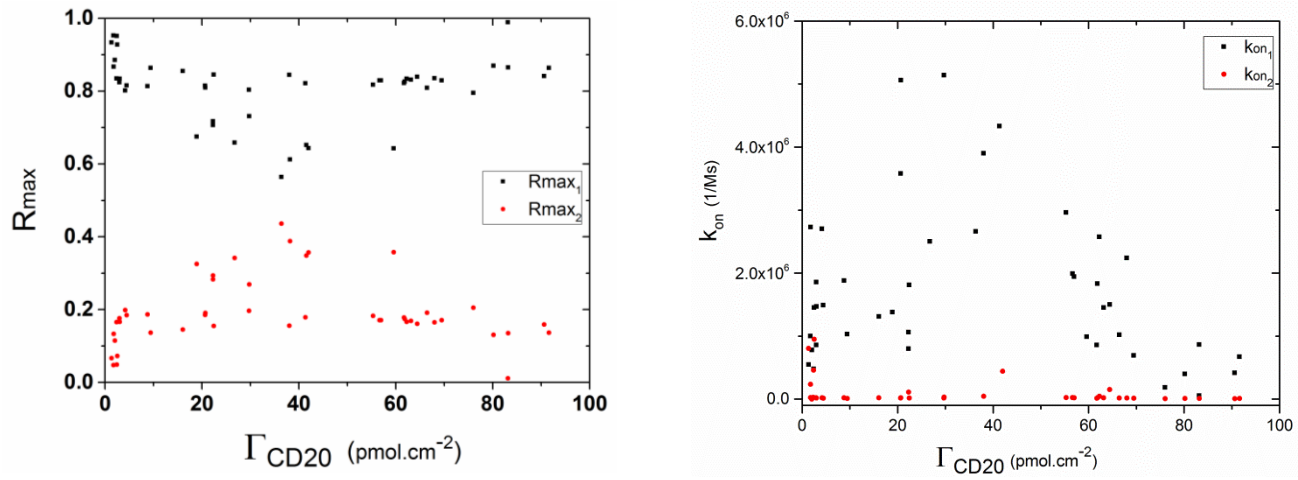

A **B**

Figure S7. (A) Normalized R_{max} (for the two interactions extracted from HL model, R_{max1}: black square, R_{max2}: red disk; normalized such that $R_{max1} + R_{max2} = 1$) as a function CD20 surface coverage. (B) Association rate constants (for the two interactions extracted from HL model, k_{on1}: black square, k_{on2}: red dot).

As the shape of the curves of the second interaction (figure S6 - insert) is characteristic of a non-specific interaction, we hypothesize that the second interaction is related to soluble RTX aggregates which can interact with the CD20 surface. This interpretation is reinforced by the variation of the normalized R_{max} with the CD20 density which is increasing for low CD20 densities (between 0 and 10 pmol.cm^{-2}). Self-association of RTX has been already mentioned in the literature and shown by using chromatography of exclusion.[4]

In conclusion, parameters related to the specific interaction are selected thanks to the magnitude and shape of the deconvolution curves.

7. SDS-PAGE analysis of Fab

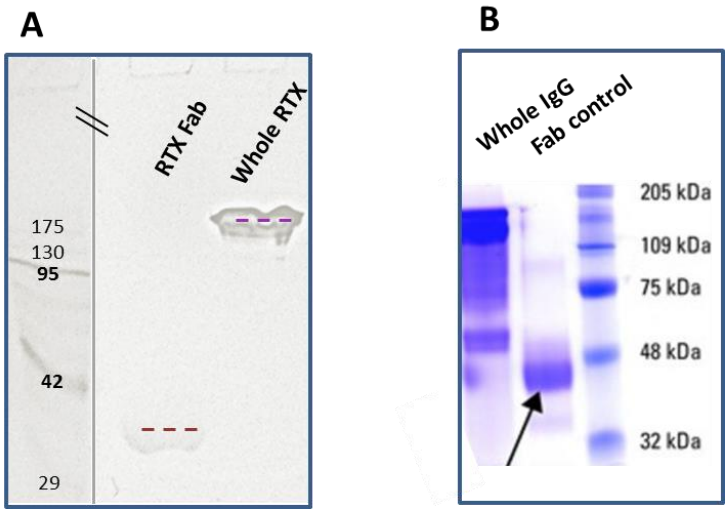

Figure S8. SDS-PAGE of IgG and its Fab fragment (A) experimental and (B) provided by Thermo Scientific.

8. Spectroscopic Ellipsometry (SE) experiments

Spectroscopic ellipsometry (SE) monitors the changes in ellipsometric angles ψ and Δ of polarized light upon reflection at a planar surface. SE is sensitive to changes in refractive index of the film and, by proper data treatment, provides access to the film refractive index and thickness, as well as the adsorbate surface density.

Experiments by QCM-D coupled with spectroscopic ellipsometry were performed in situ at a working temperature of 23 °C using a custom-designed open glass cuvette.[1] SAMs were formed on gold-coated QCM-D sensors using the same procedure as in QCM-D experiments. SE data were acquired with a spectroscopic rotating compensator ellipsometer (M2000V; J. A. Woollam, Lincoln, NE, USA) over a wavelength range of λ = 380-1000 nm, at 65° of angle of incidence. Before use, the inner surfaces of the glass cuvette were passivated by exposure to an aqueous solution of 10 $mg.mL^{-1}$ of bovine serum albumin for 10 min, rinsed with water and blow-dried with nitrogen gas. Before each experiment, measurements of the ellipsometric angles Δ and Ψ were performed on the SAM-coated surface in three distinct conditions: in air without any cuvette, in air with the sensor installed in the cuvette, and finally with the cuvette filled with ultrapure water. These steps are important to characterize SAM properties, and also to check for negligible window effects (as described in ref. 1). In situ measurements of the peptide grafting process consisted of obtaining a stable baseline in DMSO:H_2O (1:1) for a few minutes, injection of CD20 click solution at the desired final concentration, and rinsing in DMSO:H_2O (1:1) solution. During all steps, the cuvette content was continuously homogenised with the aid of a magnetic stirrer. For the rinsing step, the cuvette content was diluted by repeated addition of fresh DMSO:H_2O (1:1) solution and removal of excess liquid using a syringe needle connected to a peristaltic pump (Ismatec, Glattbrugg, Switzerland). The same procedure was performed to finally finish in water at pH 8.

The thickness and the refractive index of the layers (SAM and CD20) were determined through fitting of the data to optical models, using the software CompleteEASE (Woollam). The model relates the measured Δ and ψ as a function of λ to the optical properties of the sensor surface, the adsorbed film, and the surrounding solution. The semi-infinite bulk solution was treated as a transparent Cauchy medium, with a refractive index $nsol(\lambda) = A_{sol} + B_{sol}/\lambda 2$. For pure water as bulk solution, A_{sol} = 1.322 and B_{sol} = 0.00322 μm^2 were used. Toward determination of the thickness of the CD20 layer, the opaque gold coating modified with SAM was treated as a homogeneous substrate. Its effective optical properties were determined from data acquired in the presence of bulk solution (pure water) but in the absence of a protein film, by fitting the refractive index and extinction coefficient over the accessible λ range using a B-spline algorithm implemented in CompleteEASE. The solvated CD20 layer was treated as a single layer, which we assumed to be transparent and homogeneous (Cauchy medium), with a given thickness d and refractive index $n(\lambda) = A + B/\lambda 2$. Fitting was performed in pure water with d and A as fitting parameters, assuming B = Bsol. The $\chi 2$ value for the best fit was typically below 2, indicating a good fit. The best fit gave a CD20 layer thickness of 4.6 ± 0.2 nm and a refractive index of 1.42 ± 0.02 (for λ = 632.8 nm).

The thickness of the SAM was extracted using SE analysis in air. To this end, the surface was characterized before and after SAM formation. The optical properties of the gold coating were determined from data acquired prior to SAM formation, by fitting the refractive index and extinction coefficient over the accessible λ range using a B-spline algorithm. The SAM was treated as a Cauchy medium, and was found to be 2.5 ± 0.5 nm thick (with a refractive index of 1.29 ± 0.04, for λ = 632.8 nm).

9. QCM-D quantification of grafted peptide

Quartz crystal microbalance (QCM-D) monitors the changes in resonance frequency, Δf, and energy dissipation, ΔD, of the shear oscillation of a quartz crystal sensor upon binding and unbinding processes on the sensor surface. To a first approximation, Δf is related to the amount of bound material (including hydrodynamically coupled solvent) and ΔD is related to the softness of the interfacial film. In the case of homogeneous, quasi-rigid films the frequency shift is proportional to the mass uptake per unit area (mQCM), as described by the Sauerbrey:

$$m_{QCM} = -C\,\Delta f \qquad \text{(Eq. S2)}$$

Here, the mass sensitivity constant, C, is equal to 18.06 $ng.cm^{-2}.Hz^{-1}$ for sensors with a fundamental resonance frequency of f1 = 4.95 MHz. The areal mass density includes water hydrodynamically coupled to the organic film.

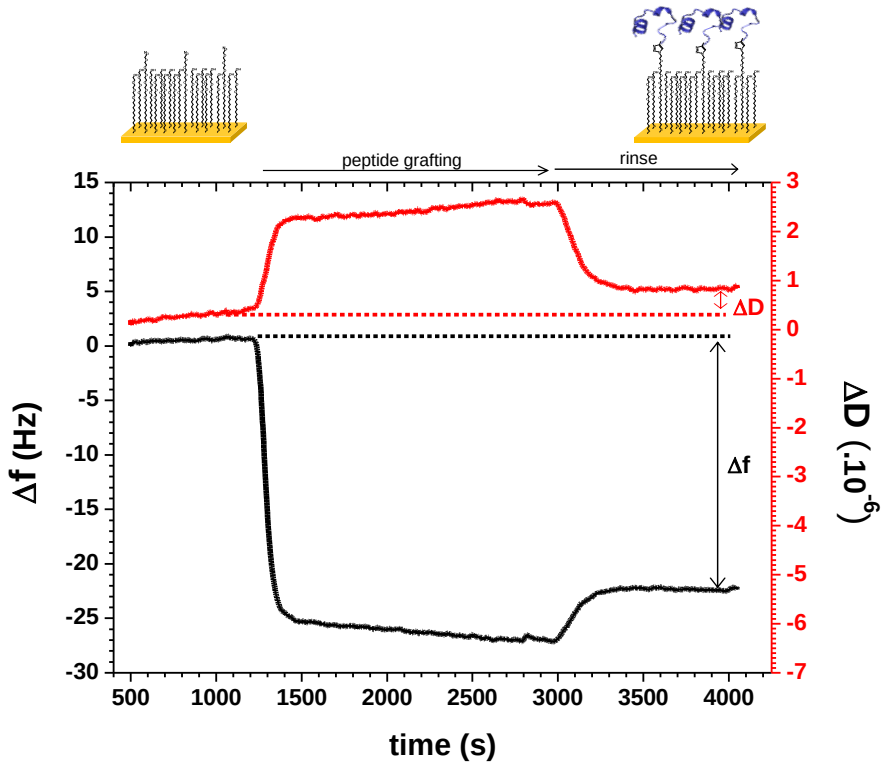

Figure S9. Example of a QCM-D profile recorded during the covalent grafting of CD20 epitope onto a SAM-azide functionalized surface prepared from a thiol mixture containing 12.5% of azide-terminated thiols. Black line: frequency shift; red line: dissipation shift. The duration of peptide grafting, and of the subsequent rinsing step, are indicated by arrows on top of the graph. A partial increase in frequency (and decrease in dissipation) is obtained when the surface is washed with the rinsing solution due to differences in the density and/or viscosity of the rinsing solution compared to the peptide grafting solution, and possibly also due to release of non-specifically bound reagents. The QCM-D signals after rinsing confirm the stability of the surface.

As expected, for a surface without azide function no measurable shift in frequency was detected when comparing before and after incubation with the CD20 antigen, signifying that there is no stable yet unspecific peptide adsorption on the surface (Fig. S7). Changes in frequency during incubation with the peptide solution are likely due to solution effects. The higher rate of change in frequency recorded during the rinsing step (compared to that of the injection step) is due to a variation of the flow rate, 5 µL/min for the injection and 20 µL/min for the rinsing.

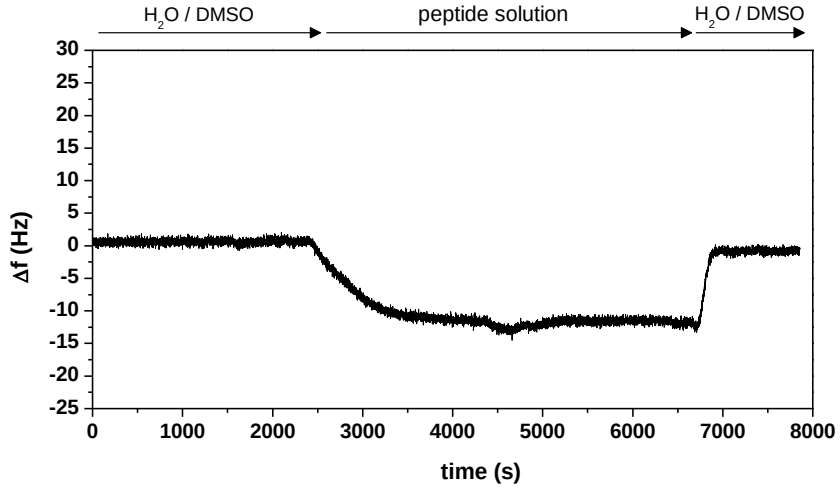

Figure S10. QCM-D profile (change in resonance frequency) characterizing the absence of CD20 grafting onto a surface without azide.

10. Calculation of the CD20 hydration layer

The hydration H of the CD20 layer is deduced from equation S3:

$H = (m_{QCM} - m_{SPR}) \times 100/m_{QCM}$ (Eq. S3)

with mSPR the optical mass (determined by Jung's formula; Eq. S1) and m_{QCM} the acoustic mass (determined with Sauerbrey's equation; Eq. S2).

11. Specificity of CD20 functionalized surface towards RTX binding – QCM-D experiment

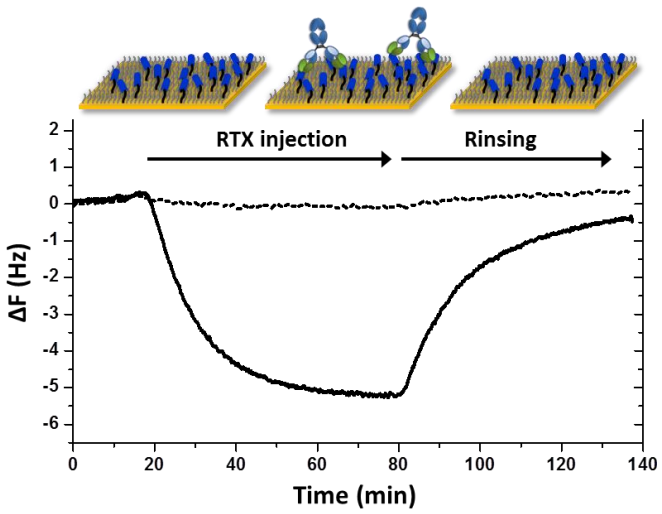

Figure S11. QCM-D profiles characterizing CD20 – RTX recognition. 10 nM RTX in phosphate buffered saline (PBS) with 3 mM citrate and 0.005% P80 was injected on 20% azide-functionalized surfaces that display CD20 (solid line) and CD20 scramble (dashed line). T = 25°C, flow rate = 10 µL.min^{-1}.

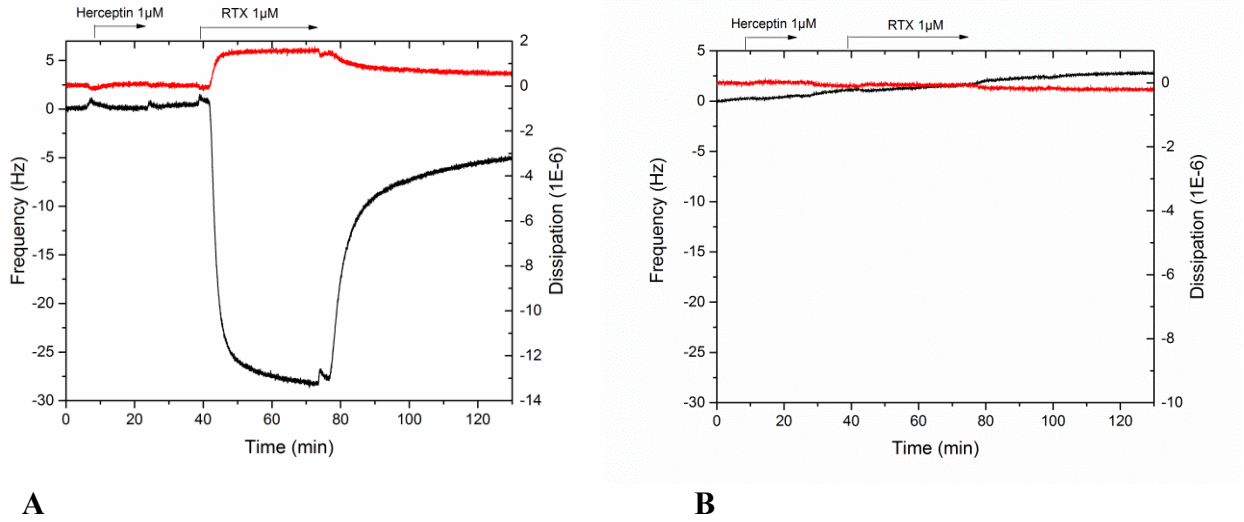

Figure S12. QCM-D profiles characterizing the specific recognition of RTX. (A) CD20 functionalized surface and (B) N_3-terminated SAM surface prepared from a thiol solution containing 10% of N_3-terminated thiol, first injection of 1µM Herceptin and second injection of 1µM RTX in phosphate buffered saline (PBS), 3 mM citrate, 0.005% P80. T = 25°C, flow rate = 10 µL.min^{-1}.

12. Calculation of the available CD20 antigens on SAM substrate

Considering the organization of the surface, it is unlikely that all CD20 antigens grafted to the surface can be fully implicated in RTX binding. Yang et al [5] have developed a model (adapted from a previous model reported by Hlavacek et al [6] characterizing the surface association in bivalent systems) with the objective of calculating the available ligand density for subsequent mAb binding to an antigen functionalized surface. According to this model some ligands may be available, whereas others are already bound in another interaction, or unavailable because they are covered by an analyte, or because a neighboring ligand obstructs binding. The probability of a ligand being available for binding can be expressed as the product of: (1) the probability that a ligand is not bound to a surface adsorbed mAb, (2) the probability that an unbound ligand is not covered by the mAb and (3) the probability that an unbound and uncovered ligand is not excluded from binding by its close proximity to a surface bound mAb.[6]

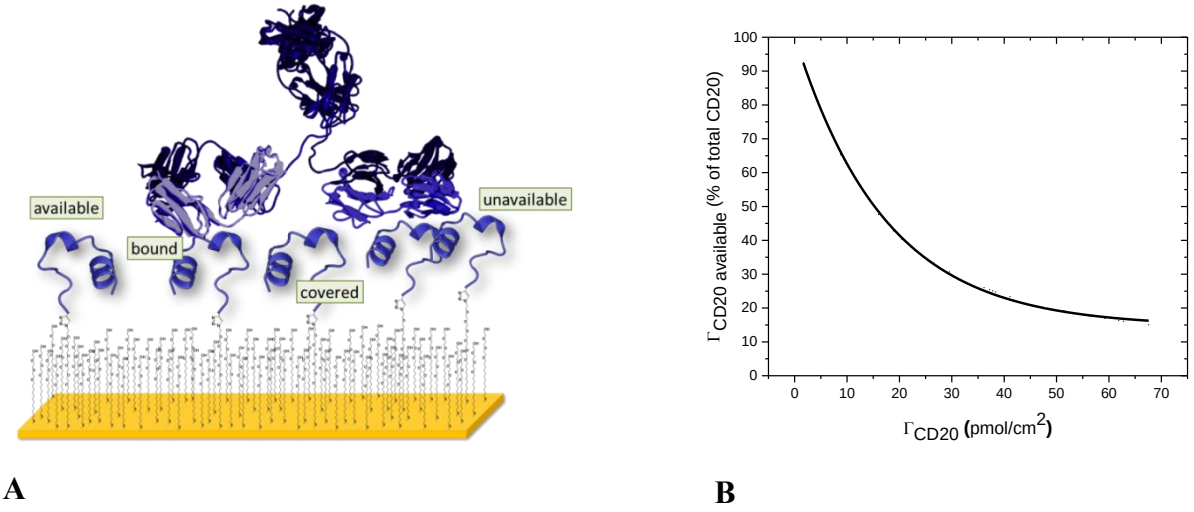

Figure S13. (A) Possible states that can be adopted by CD20 antigens on a surface; (B) Visualization of the percentage of available antigens.

The calculation of available CD20 is based on this model, where the authors calculated the probability of a ligand being available for binding when i sites are already bound. The fraction of bound sites is i/n, where n is the total number of sites. The number of i sites are calculated with equation S4.

$$i = \frac{(2 + \frac{0.5na}{A}) \pm \sqrt{4 + \left(\frac{0.5na}{A}\right)^2}}{a/A} \quad \text{(Eq. S4)}$$

where a is the area covered by an IgG antibody (60 nm^2), and n/A the density of grafted CD20 antigen calculated from SPR experiments.

The available ligand density for binding is:

$$\Gamma_{CD20}\, available = 2(n-i) + \frac{i\,a(-n+i)}{A} \quad \text{(Eq. S5)}$$

The results show that almost all CD20 are available (81%) for 1% of azide (Γ_{CD20} = 2.8 $pmol.cm^{-2}$), but only 21% are available for 12.5% (Γ_{CD20} = 46 $pmol.cm^{-2}$).

13. Determination of the binding affinity using QCM-D

The variation of KD as a function of CD20 surface densities has also been evaluated by QCM-D. To this end, RTX-CD20 binding assays were performed by QCM-D for three different azide-functionalized SAMs: 2.5, 12.5, and 50%. RTX concentrations used are:

For 2.5% thiol-azide: 10, 25, 50, 100, 250, 500, 1000, 2000 nM

For 12.5% thiol-azide: 5, 10, 50, 100, 250, 500, 1000, 2000 nM

For 50% thiol-azide: 0.05, 0.1, 0.5, 1, 2, 4, 6, 9 µM

For each RTX concentration the frequency shifts at equilibrium were plotted as a function of RTX concentration and the resulting Langmuir isotherms were fitted with equation S7 in order to obtain the apparent $K_{D,app}$.

$$\Delta f_{CD20-RTX} = \Delta f_{\max} \frac{[RTX]}{K_{Dapp} + [RTX]} \quad \text{(Eq. S6)}$$

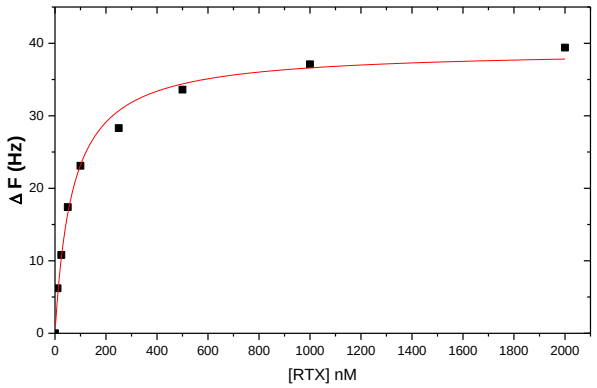

Figure S14. Example of the Langmuir isotherm obtained for the 2.5% functionalized surface.

Table S2. Comparison of CD20-RTX KD obtained from QCM-D or SPR.

% N_3	$K_{D\ \text{QCM-D}}$ (nM)	$K_{D\ \text{SPR}}$ (nM)
2.5	68.7 ± 6.8	75 ± 6
12.5	17.9 ± 3.4	32 ± 12
50	13049 ± 1372.9	1007 ± 16

As we can see in Table S2, values found in QCM-D and SPR are in the same order of magnitude in the case of surfaces with 2.5 and 12.5% of azide functions. However, the gap is more pronounced at 50%, where the K_D calculated in QCM-D is much higher (out of the concentrations injected). The trend is though still the same; and in both cases, affinity ranking is identical: K_D (12.5%) > K_D (2.5%) > K_D (50%).

14. Fab binding assays

Fab binding assays were performed in the same conditions as for RTX. Fig. S15 illustrates two sets of sensorgrams obtained for CD20 surface densities discussed in the manuscript (2.0 and 46 pmol.cm^{-2}).

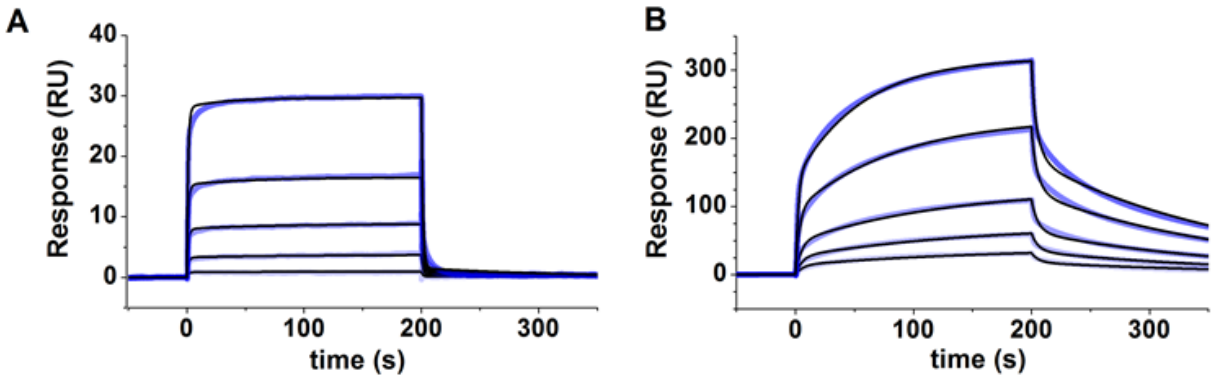

Figure S15. RTX Fab - CD20 SPR binding profiles. Sensorgrams were recorded at different CD20 surface densities: (A) 2.8 pmol.cm^{-2}, and (B) 46 pmol.cm^{-2}. The Fab fragment concentrations were 50, 200, 500, 1000 nM for 2.8 pmol.cm^{-2}, and from 50, 100, 200, 500, 1000 nM for 46 pmol.cm^{-2}. The sensorgrams were fitted with the heterogeneous ligand kinetic model (RI correction = 0) and the fitted curves were added to the graph (black curves).

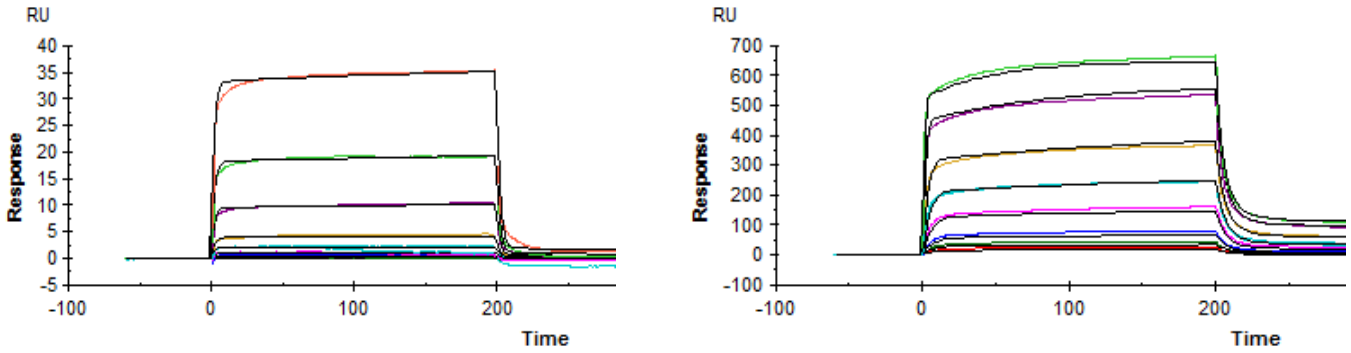

(A) RTX Fab-CD20 SPR binding profiles (colored curves), black curves are the fitted curves (heterogeneous ligand kinetic model: k_a= 0.5 10^5 $M^{-1}.s^{-1}$)

(B) RTX-CD20 SPR binding profiles (colored curves), black curves are the fitted curves (heterogeneous ligand kinetic model: ka=18.5 10^5 $M^{-1}s^{-1}$)

Figure S16. Examples of sensorgrams recorded on the same CD20 functionalized sensor chip bearing 2.8 pmol.cm^{-2} (prepared from thiol solution containing 1% of azide) for Fab fragment (A) and for RTX (B) concentrations of 5, 10, 20, 50, 100, 200, 500, 1000 nM.

15. References

1. Jung, L. S.; Campbell, C. T.; Chinowsky, T. M.; Mar, M. N.; Yee, S. S. *Langmuir* **1998**, *14*, 5636–5648.
2. a) Dejeu, J.; Bonnet, H.; Spinelli, N.; Defrancq, E.; Coche-Guerente, L.; Van der Heyden, A.; Labbé, P. *J. Phys. Chem. C* **2018**, *122*, 21521-21530 ; b) Mac Donald, H.; Bonnet, H.; Van der Heyden, A.; Defrancq, E.; Spinelli, N.; Coche-Guérente, L.; Dejeu, J. *J. Phys. Chem. C* **2019**, *123*, 13561-13568.
3. Schoch, R. L.; Kapinos, L. E.; Lim, R. Y. H. *Proc. Natl. Acad. Sci.* **2012**, *109*, 16911–16916.
4. Morgan, H.; Tseng, S.-Y.; Gallais, Y.; Leineweber, M.; Buchmann, P.; Riccardi, S.; Nabhan, M.; Lo, J.; Gani, Z; Szely, N.; Zhu, C. S.; Yang, M.; Kiessling, A.; Vohr, H.-W.; Pallardy, M.; Aswad, F.; Turbica, I. *Front. Immunol.* **2019**, *10*:601. doi: 10.3389/fimmu.2019.00601.
5. Yang, T.; Baryshnikova, O. K.; Mao, H.; Holden, M. A.; Cremer, P. S. *J. Am. Chem. Soc.* **2003**, *125*, 4779–4784.
6. Hlavacek, W. S.; Posner, R. G.; Perelson, A. S. *Biophys. J.* **1999**, *76*, 3031–3043.